Positron-impact ionization, positronium formation, and electronic excitation cross sections for diatomic molecules

J. P. Marler and C. M. Surko

Department of Physics, University of California, San Diego, 9500 Gilman Drive, La Jolla, California 92093-0319, USA

Absolute measurements are presented for the positron-impact cross sections for positronium formation, direct ionization, and total ionization of the diatomic molecules N_2, CO, and O_2, in the range of energies from threshold to 90 eV. Cross sections for the electronic excitation of the $a\ ^1\Pi$ and $a'\ ^1\Sigma$ state in N_2 and the $A\ ^1\Pi$ state in CO near threshold are also presented. The experiment uses a cold, trap-based positron beam and the technique of studying positron scattering in a strong magnetic field. In O_2, a feature previously seen in the total ionization cross section is observed in both the positronium formation and total ionization cross sections. The possible origin of this feature and its relationship to positron-induced dissociation is discussed. In N_2, the near-threshold electronic excitation cross section is larger than that for positronium formation. This likely explains the relatively high efficiency of this molecule when used for buffer-gas positron trapping.

I. INTRODUCTION

We have recently used a trap-based positron beam to measure the cross sections for positronium formation, direct ionization, and total ionization for noble gas atoms [1]. In the work presented here, this method is used to make similar measurements for the diatomic molecules N_2, CO, and O_2. These targets are interesting for several reasons. Comparison of N_2 and CO is of interest because these molecules are isoelectronic. For N_2 and O_2, new calculations of the cross sections for direct ionization are available [2,3]. Finally, the data reported here include measurements of the positronium formation cross sections for N_2 and CO, and improved measurements for O_2.

The formation of positronium Ps (i.e., the "atom" consisting of a bound electron-positron pair) is relevant, for example, to applications in a variety of fields including material science and biophysics. Since there is no analog of positronium formation in electron scattering, the extensive understanding of electron interactions with atomic targets is of little help in developing procedures to treat this phenomenon theoretically. In particular, positronium formation requires the inclusion of an additional set of final states. This poses a serious challenge to theory that has not yet been solved in general, particularly at lower values of positron energy where simple perturbative approaches, such as the Born approximation, are invalid.

Also presented are state-resolved measurements of the positron-impact excitation of the lowest-lying electronic states in CO and more detailed measurements for N_2. There has been very little theoretical work to date on the positron-impact excitation of these and similar molecular targets. It is hoped that the data presented here will motivate further efforts to understand these important processes. The synthesis of the ionization data with the electronic excitation measurements provides a more complete picture of low-energy positron excitation processes for these targets.
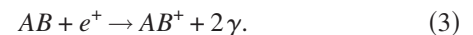
Positrons can ionize a diatomic molecule AB (or A_2, depending on the molecule) by three processes: direct ionization

$$AB + e^+ \rightarrow AB + e^+ + e^-; \tag{1}$$

positronium formation

$$AB + e^+ \rightarrow AB^+ + Ps; \tag{2}$$
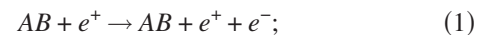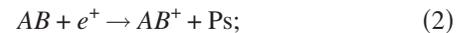
and direct annihilation

$$AB + e^+ \rightarrow AB^+ + 2\gamma. \tag{3}$$

The first two processes have cross sections on the order of a_0^2, where a_0 is the Bohr radius, whereas the latter has a cross section that is orders of magnitude smaller [4]. Thus, to a good approximation,

$$\sigma_{TI} = \sigma_I + \sigma_{Ps}, \tag{4}$$

where σ_{TI} is the total ionization cross section, σ_I is the direct ionization cross section, and σ_{Ps} is the positronium cross section.

In addition to the ionization processes described by Eqs. (1)–(3), and positron-impact electronic excitation of a molecule, one more reaction is relevant to the work presented here, that of positron-induced dissociation,

$$AB + e^+ \rightarrow A + B + e^+, \tag{5}$$
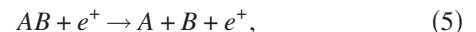
where one or both of the atoms, A and B, can be in an excited electronic state.

The measurements presented here are made with a cold, trap-based positron beam. Scattering is studied in a strong magnetic field, which permits absolute measurements of the scattering cross sections without need for normalization to other cross sections. Measurements are presented for direct and total ionization and positronium formation in the diatomic molecules N_2, CO, and O_2. The measured direct ionization cross sections for all three diatomic molecules are similar. In the case of positronium formation, the N_2 and CO cross sections have similar magnitudes and features; however, in O_2, the cross section is lower by approximately a factor of 2 and contains a feature close to threshold not observed in either N_2 or CO. The possibility that this feature is due to the distribution of valence-electron positronium for-
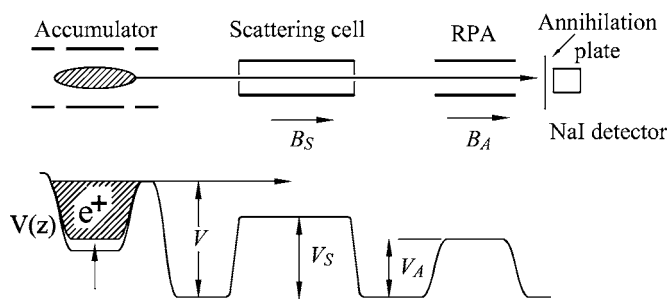
FIG. 1. Schematic diagram of the electrode structure (above) and the electric potentials (below) used to study scattering with a trap-based positron beam. The positron beam is guided by an applied magnetic field of strength B_S in the scattering cell and B_A in the retarding potential analyzer (RPA).

mation thresholds in O_2 and a positron-induced dissociation channel is discussed.

Also presented are state-resolved electronic excitation cross section measurements for CO and higher-resolution measurements for N_2. The absolute magnitude of the cross section for the $A\,^1\Pi$ excited state in CO is approximately a factor of 2 larger than that for the corresponding state in N_2. In the case of N_2, the electronic excitation cross section near threshold is larger than the cross section for positronium formation, whereas this is not true in CO. It is likely that the large near-threshold electronic excitation cross section in N_2 is the reason that N_2 is the buffer gas of choice for efficient positron trapping [5,6].

II. EXPERIMENTAL TECHNIQUES

A. Trap-based positron beam and scattering apparatus

The experimental technique for forming a cold, trap-based positron beam has been described in detail previously [7,8]. Positrons from a ^{22}Na radioactive source and neon moderator are trapped and cooled in a three-stage buffer-gas Penning-Malmberg trap in a 0.15 T magnetic field. The positrons cool to the temperature of the buffer gas and surrounding electrodes (i.e., 300 K $\equiv$ 25 meV) in $\sim$0.1 s.

The process of positron beam formation is illustrated schematically in Fig. 1. Following a cycle of positron trapping and cooling, the electric potential in the accumulator is carefully raised to force the positrons out of the trap at a well defined energy, set by the potential V in Fig. 1. In order to maintain good energy resolution, the positron beam is operated in a pulsed mode with bursts of $\sim$15 000 positrons generated at a 4 Hz rate. The beam energy in the gas cell, $\epsilon = e(V - V_S)$, where V_S is the potential in the scattering cell, can be varied from $\sim$0.05 to 100 eV. Differential pumping isolates the buffer-gas trap from the scattering experiment. Positron pulses are passed through the scattering cell which contains the test gas. Positrons that have not annihilated or formed positronium in the scattering cell are guided by the magnetic field through a cylindrical retarding potential analyzer (RPA) electrode, and finally to a metal plate where the positrons annihilate. The magnetic field in the scattering cell, B_S, is 0.09 T. The magnetic field in the RPA, B_A, is adjust-
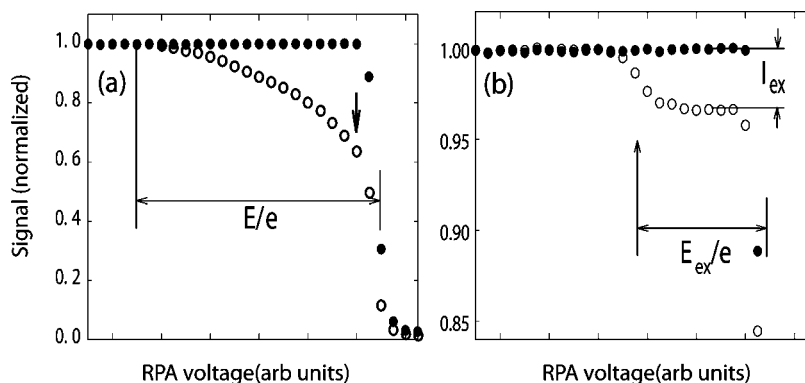
able from zero to 0.09 T. The resulting γ rays from the annihilation plate are monitored using an NaI crystal and photomultiplier.

The gas cell is 38.1 cm long and 7.0 cm in diameter, with entrance and exit apertures 0.5 cm in diameter. Cylindrical mesh grids inside the cell at the entrance and exit are used to further tune the potential to be constant near the entrance and exit of the cell. The electrical potential V_A on the RPA can be varied to analyze the energy distribution of the positrons that pass through the scattering cell. The RPA is also used to analyze the incident energy distribution of the positron beam (i.e., with the test gas removed from the scattering cell). The energy resolution of the positron beam used in the experiments described here is $\sim$25 meV (full width at half maximum). The apparatus achieves this vacuum environment by the use of cryopumps. The base pressure of the scattering apparatus is $\sim$5 $\times$ 10^{-8} torr.

B. Scattering measurements using a strong magnetic field

The cross section measurements presented here were done using a technique that relies on the fact that the positron orbits are strongly magnetized [9,10]. In a strong magnetic field, namely, where the positron's gyroradius is small compared to the characteristic dimensions of the scattering apparatus (but still large compared to atomic dimensions), the total kinetic energy is separable into two components: energy in motion parallel to the magnetic field, $E_\parallel$, and that in the cyclotron motion in the direction perpendicular to the field, $E_\perp$. For the experiments described here, the magnetic field in the scattering region, B_S, and in the analyzing region, B_A (see Fig. 1), can be adjusted independently. This then allows us to take advantage of the adiabatic invariant $\xi = E_\perp / B$. To a good approximation, ξ is constant in the case relevant here, namely, when the magnetic field is strong in the sense described above, and the field varies slowly compared to a cyclotron period in the frame of the moving positron.

If a positron is scattered in the gas cell, then some of the positron's energy will be transferred from the parallel to the perpendicular component, with the specific amount depending on the scattering angle. The integral cross section measurements reported here rely on the fact that, by reducing the magnetic field in the analyzing region, most of the energy in $E_\perp$ can be transferred back into $E_\parallel$ (due to the fact that ξ is constant), while the total kinetic energy of the positron remains constant. In the current experiments, the magnetic field ratio M between the scattering cell and RPA is 35:1, which is sufficient to ensure that the value of $E_\parallel$ in the region of the RPA is, to a good approximation, equal to the total kinetic energy of the positron at that location. Thus the difference between the incident positron energy and that measured by the RPA is an absolute measure of the energy lost due to inelastic scattering. This procedure provides an accurate method with which to make integral inelastic cross section measurements [11,12]. Absolute cross sections are obtained by normalizing the transmitted signal to the incident beam strength. This avoids the need to normalize the measurements to other cross sections, as has typically been done previously for ionization and total cross section measurements [13].

FIG. 2. Example of the method used to determine integral-inelastic and total cross sections: positron scattering from CO. Shown are normalized RPA data for positrons going through the scattering cell (●) with no gas in the scattering cell, and (○) with CO in the scattering cell, for (a) a magnetic field ratio $M=1$; and (b) $M=35$. The vertical arrow in (a) denotes the point used to measure the total scattering cross section. The height of the step in the curve, I_{ex}, in (b) is proportional to the integral cross section for the vibrational excitation of CO ($E_{ex}=0.27$ eV) [11]. Note the expanded vertical scale in (b).

C. Cross sections for specific processes

In this paper, we use the method described above to measure absolute electronic excitation and direct ionization cross sections for diatomic molecules. Positronium formation cross sections are measured as a loss of positrons from the incident beam. An example of data used to determine integral inelastic scattering cross sections is shown in Fig. 2 for the case of vibrational excitation of CO. The integral inelastic scattering cross section is determined by the equation

$$\sigma_{ex}(\epsilon) = \frac{1}{n_m l} \frac{I_{ex}(\epsilon)}{I_0}, \qquad (6)$$

where n_m is the number density of the target gas, and l is the path length. $I_{ex}(\epsilon)$ corresponds to the number of positrons undergoing the excitation process (i.e. the step height), and I_0 corresponds to the total number of positrons in the initial pulse (e.g., one unit in the normalized data shown in Fig. 2).

In Eq. (6) and elsewhere in this paper, we assume the weak-scattering limit of the Lambert-Beer law, namely, that the fraction of scattered particles $\Delta I \ll I_0$. The total cross section for each target atom was measured in order to determine the appropriate operating pressure to be consistent with this assumption. The total scattering is proportional to the decrease in the transmitted beam when the RPA is set just below the beam cutoff energy with the mirror ratio between the scattering cell and RPA set at $M=1$ [i.e., see arrow in Fig. 2(a)] [10]. The test-gas pressure was chosen such that the probability of undergoing a single collision in the scattering cell was less than 15%. This corresponded to target gas pressures in the range of 0.05–0.5 mtorr for the target species studied. The main source of error in the data is statistical.

The apertures on the scattering cell are sufficiently small so that there is a well defined interaction region where the gas pressure and the electric potential are constant, and therefore the interaction path length can be accurately determined. In all cases, the test gas pressure was measured using a capacitance manometer with an expected error below 1%.

This accurate knowledge of the pressure and path length and Eq. (6) allows us to make absolute cross section measurements. For the results in this paper, the following equation was used which incorporates the known geometry:

$$\sigma_{ex}(\epsilon) \ (a_0^2) = \frac{P \ (\text{mtorr})}{28.6} \frac{I_{ex}(\epsilon)}{I_0}, \qquad (7)$$

where P is the pressure in mtorr and the cross section σ_{ex} is given in units of a_0^2 where a_0 is the Bohr radius. Equation (7) is the general expression for calculating inelastic scattering cross sections.

D. Electronic excitation

The RPA curves for electronic excitation of molecules exhibit a more complicated structure than for the vibrational excitation of molecules [cf. Fig. 1(b)] or the electronic excitation of atoms. This structure is the result of the fact that, associated with each electronic transition is a manifold of vibrational transitions. An example of a retarding potential curve for the case of positrons incident on N$_2$ is shown in Fig. 3 [12].

The experimental energy resolution provided by the trap based beam allows us to resolve the vibrational manifold
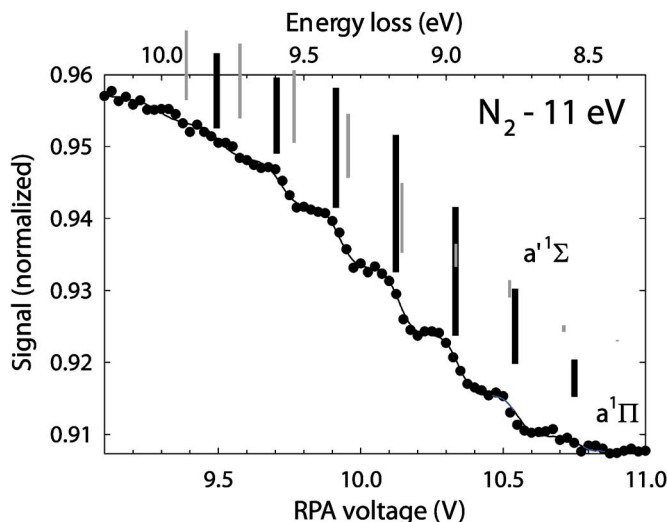

FIG. 3. (Color online) Raw data for electronic excitation in N$_2$. The positron energy in the scattering cell is 11 eV, and the beam transport energy (set by V in Fig. 1) is 19.3 eV. The positions of vibrational manifold energies for each electronic state are shown as vertical bars. The lengths of the bars are proportional to the Franck-Condon factor for each transition and therefore show the relative weighting of the vibrational states within an electronic state.

associated with a given electronic transition [12]. In the case of the molecules studied here, there is a further complication. The observed RPA curve is the sum of overlapping step functions for different electronic transitions. Fortunately, we are able to use the fact that the relative heights of the vibrational steps for each electronic transition have been calculated. These values, namely the so-called Franck-Condon factors, are the transition probabilities for the excitation from the ground state to a specific vibrational state within a particular excited state manifold.

By using the known Franck-Condon factors for the vibrational manifold for each electronic state, the cross sections for excitation of the individual electronic states can be deduced. This is done by fitting the data to an expression consisting of a series of summed, resolution-broadened error functions representing the energetically accessible vibrational levels [12]. The relative magnitudes of the step heights are set by the Franck-Condon factors. The solid line in Fig. 3 is an example of such a fit for N_2. The absolute step heights are proportional to the cross sections for this process. Reference [14] gives the Franck-Condon factors for N_2. For CO we used the values calculated by Cartwright [15].

E. Direct ionization

For direct ionization measurements, the RPA is set to exclude positrons that have lost an amount of energy corresponding to the ionization energy or greater. As a result, only positrons that have lost less than this amount of energy pass through the RPA to the detector. The difference between the signal strength when the RPA is set to allow all of the positrons to pass through the RPA and that when the RPA is set to reject those that have ionized the test species is denoted as I_I.

The incident beam strength I_0 is measured by ensuring that the positron energy inside the gas cell is below the threshold for positronium formation (i.e., the ionization energy minus the positronium binding energy 6.8 eV). This measurement is taken with the test gas in the scattering cell. Positrons that backscatter in the cell are reflected from the back wall of the trap and sent back toward the detector.

The absolute, direct ionization cross section is then given by the equation

$$\sigma_I(\epsilon) = \frac{1}{n_m l} \frac{I_I(\epsilon)}{I_0}, \qquad (8)$$

where $I_I(\epsilon)$, as defined previously, is the magnitude of the loss in signal strength due to ionization by positrons with energy ϵ in the gas cell, n_m is the number density of the target gas, and l is the path length in the scattering cell.

F. Positronium formation

Since positronium is a neutral atom, positrons that form positronium in the scattering cell are not guided by the magnetic field, and the vast majority are therefore lost before striking the detector. Positronium lifetime aside, the solid angle $\delta\Omega$ of the annihilation plate as viewed from the gas cell through the exit aperture of the cell is negligibly small, $\delta\Omega < 10^{-3}$. Positrons either annihilate in the scattering cell

TABLE I. Characteristic energies for N_2 and CO and O_2 [19].

Molecule	Excitation	Ps formation	Direct ionization
N_2	8.59 eV[a]	8.78 eV	15.58 eV
CO	8.07 eV[a]	7.21 eV	14.01 eV
O_2	7.05 eV[b]	5.4 eV	12.2 eV

[a]Electronic, $^1\Pi$ state.
[b]Threshold for dissociation to atomic oxygen (Schumann-Runge band).

because of the short annihilation lifetime of the Ps atom (i.e., 0.12 ns for para-positronium and 142 ns for ortho-positronium), or drift out of the beam and annihilate at the walls of the cell. In either case, positronium formation results in a loss of positron beam current. In the case of the magnetically guided positron beam used here, all positrons that do not form positronium, including those backscattered in the scattering cell [10], will be transmitted through the RPA (which is grounded during these measurements) and strike the detector plate. Those positrons that are backscattered will reflect off of the exit gate of the buffer gas trap, then travel through the scattering cell a second time, before arriving at the detector.

The difference between the incident beam strength I_0 and the transmitted beam strength when the positron has energy ϵ in the gas cell is denoted as $I_{Ps}(\epsilon)$ and is proportional to the number of positronium formed at that energy. The only other possible positron loss process is so-called direct annihilation. Since the cross section for direct annihilation at the energies studied is orders of magnitude smaller than that for positronium formation, this contribution is neglected.

The positronium formation cross section is then given by

$$\sigma_{Ps}(\epsilon) = \frac{1}{n_m l} \frac{I_{Ps}(\epsilon)}{I_0}, \qquad (9)$$

where n_m and l are defined above. The quantity I_0 is measured as the incident beam strength with gas in the cell and with the positron energy in the cell less than the threshold for positronium formation. The total ionization cross section is calculated as the sum of the direct ionization and positronium formation cross sections.

III. EXPERIMENTAL RESULTS

In this section, we describe results for direct ionization, positronium formation, and total ionization in N_2, CO, and O_2. We also describe measurements for positron-impact excitation of the lowest-lying electronic excited states of N_2 and CO. Relevant energies for these processes are summarized in Table I.

A. Ionization: N_2 and CO

Figure 4 shows the current measurements for Ps formation, direct ionization, and total ionization cross sections for N_2. Similar to the noble gases, the positronium formation
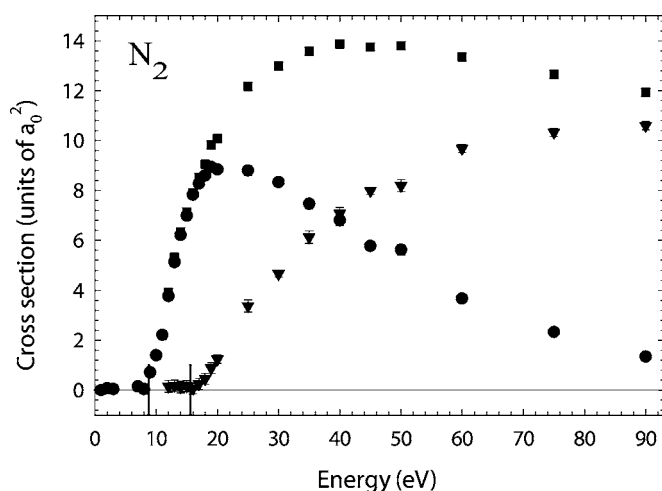
FIG. 4. Integral cross sections for N_2: (●) positronium formation, (▼) direct ionization, and (■) total ionization. Vertical bars in this and subsequent figures mark the positions of the Ps formation and direct ionization thresholds.

cross section in N_2 has a sharp turnon. The positronium formation cross section peaks around 20 eV, slightly past the threshold for direct ionization.

Figure 5 shows the present data for N_2 compared with other recent experimental results for the direct and total ionization cross sections [16]. To our knowledge, there are no other published results for the positronium formation cross section in N_2. The current direct ionization measurements are slightly larger than the only other measurements of this cross section (i.e., those shown in Fig. 5). The current total ionization cross section, on the other hand, is about a third smaller than those reported in Ref. [16]. The origin of this significant discrepancy is not presently understood.

Also shown in Fig. 5 is the Coulomb plus plane waves, full energy range (CPE) distorted wave calculation of Cam-
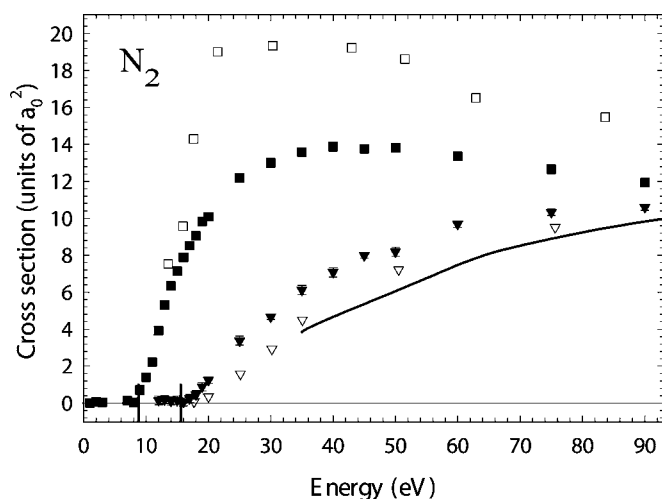

FIG. 5. Integral cross sections for N_2: (▼) direct ionization and (■) total ionization cross section. Shown for comparison are the experimental results of Ref. [16] for (▽) direct ionization and (□) total ionization. The CPE theoretical result of Ref. [2] for direct ionization is shown by the solid line.
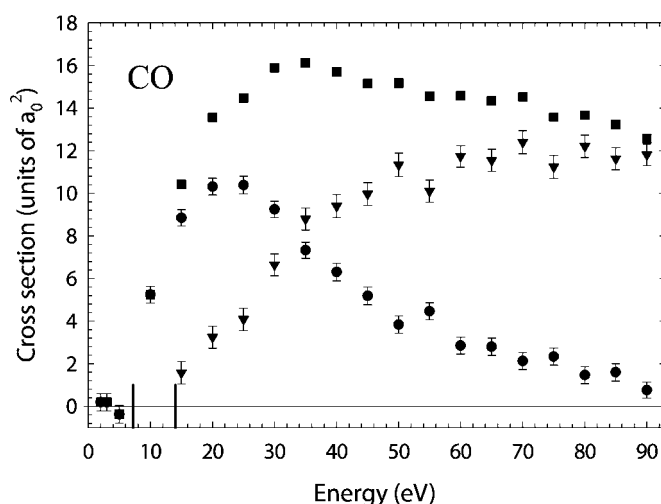

FIG. 6. Integral cross sections for CO: (●) positronium formation, (▼) direct ionization, and (■) total ionization.

peanu [2]. The CPE method includes the full Coulomb interaction between the slower of the two outgoing particles (the scattered positron or the ejected electron) and the residual target ion while the fast outgoing particle is described by a plane wave. Using energy-dependent combinations of the static potentials of the neutral atom and the residual ion, this calculation accounts, at least approximately, for the partial screening of the ionic charge by each of the two outgoing particles. The positronium formation channel is not included in these calculations. Given the simplicity of the model, the theoretical results are in reasonably good agreement with the measurements.

Figure 6 shows the current measurements in CO for the cross sections for the Ps formation, direct ionization, and total ionization cross sections. The positronium formation and direct ionization cross sections are similar in shape and magnitude to those of N_2. There is a similar sharp onset in the positronium formation cross section which peaks around 24 eV. The direct ionization cross section has a slower rise than that for positronium formation and flattens out somewhat near the end of the range of energies studied similar to that in N_2.

Figure 7 compares the present results for CO with other recent experimental results for the direct and total ionization cross sections [17]. Both of the current direct and total ionization cross sections are in reasonably good agreement with those of Ref. [17]. As in N_2, at lower energies (e.g., <60 eV) the current measurements for direct ionization are systematically higher than those of Ref. [17] but the two sets of data are in better agreement at higher energies. Also shown in Fig. 7 is the CPE distorted-wave calculation of Campeanu [18]. Similar to the case of N_2, given the simplicity of the model, the theoretical predictions are in reasonably good agreement with the measurements.

B. Ionization: O_2

1. Direct ionization and positronium formation

Shown in Fig. 8 are the results of the current measurements of the cross sections for positronium formation, direct
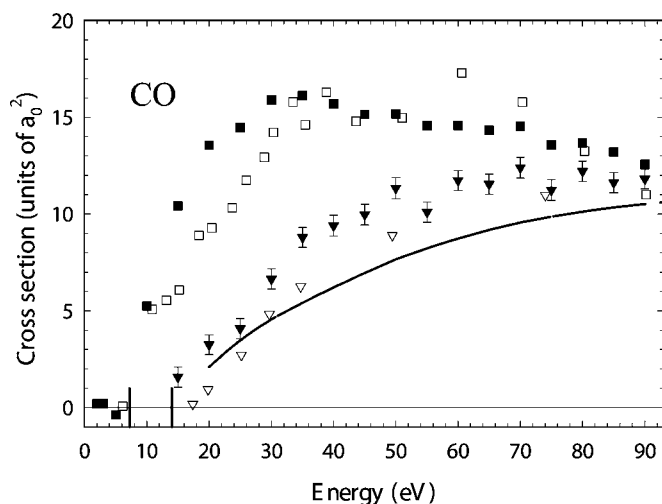
FIG. 7. Present measurements of the integral cross sections for CO: (▼) direct ionization and (■) total ionization. Shown for comparison are the experimental results of Ref. [17] for (▽) direct ionization and (□) total ionization and theoretical calculation (—) of Ref. [18]. Vertical bars mark the positions of the Ps formation and direct ionization thresholds.

FIG. 9. Present measurements of the integral cross section for (▼) direct ionization in O_2. Also shown for comparison are the experimental results of (▽) [20], and the theoretical calculation of (− −) [3]. Vertical bars mark the positions of the Ps formation and direct ionization thresholds.

ionization and total ionization for O_2. The direct ionization cross section is similar in shape and magnitude to those of N_2 and CO. The positronium formation cross section, on the other hand, is distinctly different than those observed for the other two molecules with a magnitude about 2/3 of that observed in N_2 and CO. The O_2 cross section has a sharp rise at threshold followed by a dip in the cross section before a more gradual rise to the main peak in the cross section at about 18 eV.

In Fig. 9, the present results for direct ionization in O_2 are compared to the experimental results of Ref. [20] and the predictions of the distorted-wave model CPE theoretical calculations of Campeanu *et al.* [3]. While both sets of experimental data are in excellent agreement, the measurements are significantly larger than the theoretical predictions.

Figure 10 compares the present data for O_2 with other recent experimental values for the total ionization and posi-
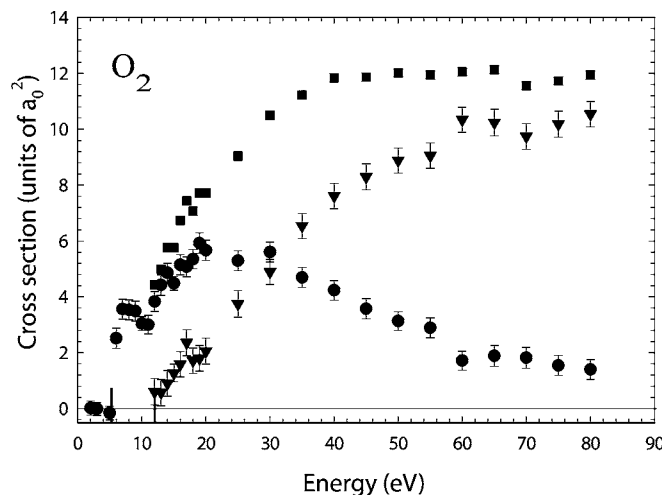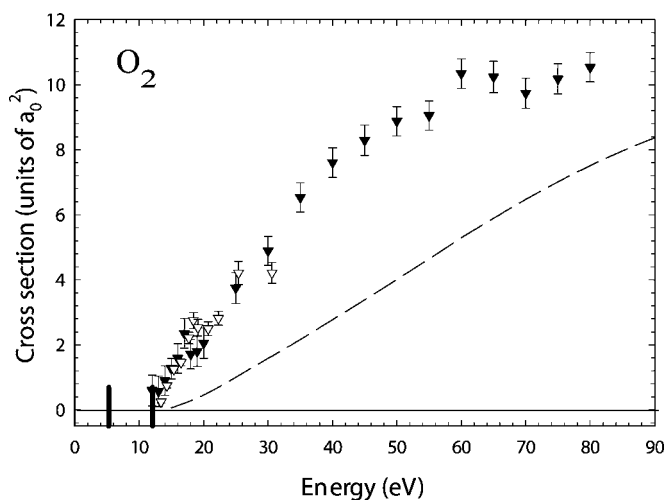
tronium formation cross sections. The present values for the positronium formation cross section are in good agreement with those of Ref. [22] from the positronium formation threshold to the threshold for direct ionization (i.e., from 5 to 12 eV). In contrast, at higher energies, the values from Ref. [22] are lower than the current measurements by a factor of ∼1.5–2. The situation for the total cross section is somewhat the opposite. While the values of the total cross section from Ref. [21] agree with the present measurements
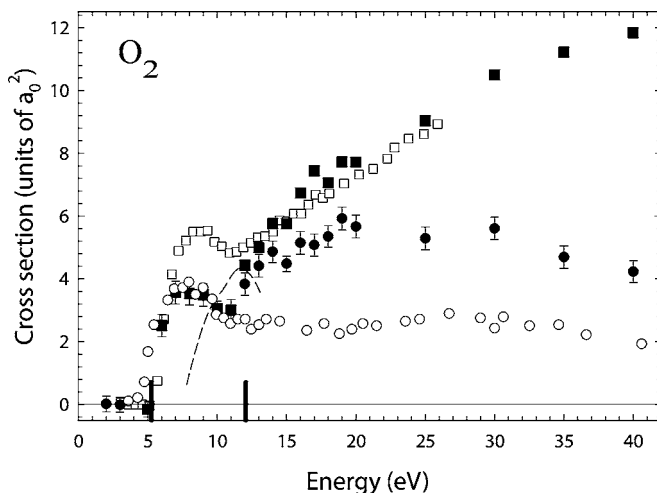

FIG. 10. Present measurements of the integral cross sections for O_2: (●) positronium formation and (■) total ionization cross section. Below the direct ionization threshold at 12.07 eV, the value of the positronium formation and total ionization cross sections are equal. Also shown for comparison are the experimental results for (□) the total ionization from Ref. [21]; and (○) positronium formation from Ref. [22]. Vertical bars mark the positions of the Ps formation and direct ionization thresholds. The experimental cross section for the excitation to the Schumann-Runge continuum from Ref. [20] is also shown (--). See text for details.

FIG. 8. Integral cross sections for O_2: (●) positronium formation, (▼) direct ionization, and (■) total ionization.

up to ~7 eV, they are higher than the current measurements from 7 eV to just above the threshold for direct ionization at 12 eV. Above the direct ionization threshold, there is again good agreement between these two independent total ionization cross section measurements.

With regard to the discrepancy between the current Ps formation data and that from Ref. [22] above the threshold for direct ionization, we note that we can make a second, independent determination of the Ps formation cross section in this region of energies by subtracting our direct ionization measurements from the total ionization measurements of Ref. [21]. The result agrees well with our Ps formation measurements. Thus this analysis confirms the present Ps formation measurements relative to those of Ref. [22] where they disagree above 12 eV. In the next section, we discuss further the differences between the total ionization cross section of Ref. [21] and the current Ps formation measurements in the range from 6 to 12 eV.

2. Unusual near-threshold behavior in O_2

As compared to N_2 and CO and noble gas atoms [1], the present Ps formation data in O_2 exhibit unusual near-threshold behavior. As shown in Fig. 10, there is a very sharp rise at threshold, immediately followed by a sharp change in slope and gradual decrease in the cross section from about 7 to 11 eV. A similar feature was seen previously in the total cross section measurements of Laricchia *et al.* [21]. In their work, they suggested that the correspondence between the dip in their total ionization data around 11 eV and the increase in the cross section around 12 eV is the result of a coupling between the Ps formation and a well-known dissociation channel in O_2. In particular, the experimental cross section for positron excitation of the Schumann-Runge (SR) bands and continuum in O_2 is shown by the dashed line in Fig. 10 [20]. These bands correspond to transitions from the ground state, $^3\Sigma_4^-$, to the $^3\Sigma_u^-$ state. They begin at 6.2 eV and converge to a limit at 7.05 eV that is followed by a continuum corresponding to the reaction [19]

$$O_2 + e^+ \rightarrow O(^3P) + O(^1D) + e^+. \qquad (10)$$
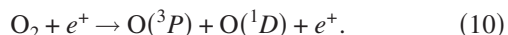
The present data also exhibit a change in the slope of the total ionization cross section around 7 eV and a dip around 11 eV (i.e., in approximately this same region of energies). It seems plausible that these somewhat atypical features could be due to the O_2 dissociation channel.

However, O_2 also differs from N_2, for example, in another respect. In oxygen, there is a larger gap in energy between Ps formation on the highest-lying molecular orbital and the next set of orbitals. The Ps threshold for the highest-lying molecular orbital in O_2 is 5.27 eV (two electrons), and the thresholds for the other orbitals are at 9.29 eV (four electrons) and 11.36 eV (two electrons) [23], close to the start of the increase in the present Ps formation data at ~12 eV. This relatively large gap in Ps formation thresholds likely contributes to the relatively flat slope in the Ps formation cross section above 7 eV.

There does remain, however, a discrepancy at energies between 6 and 12 eV between the two independent sets of Ps formation data (i.e., the present data and those from Ref.
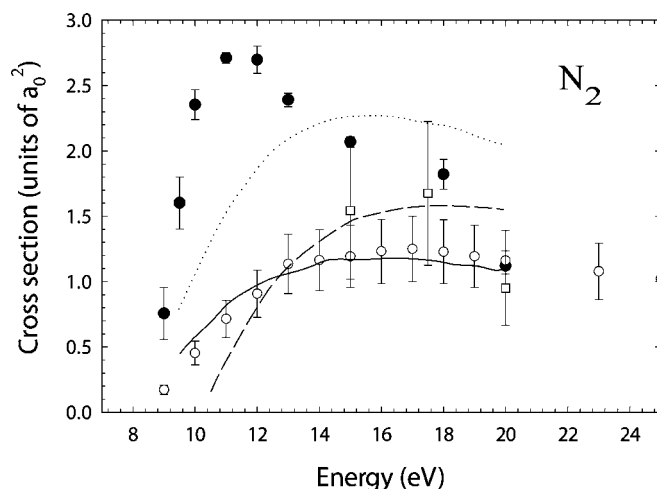

FIG. 11. Integral cross sections in N_2 for the excitation of the $a\ ^1\Pi$ states by ($\bullet$) positrons and ($\bigcirc$, $\square$) [24,25] electrons. Also shown are the three theoretical predictions for positron excitation of the $a\ ^1\Pi$ state from Ref. [26]. All curves were calculated using the Schwinger multichannel formalism with different choices for the basis sets: (—) mixed antibonding orbitals, (···) mixed bonding orbitals, and (--) Hartree Fock orbitals.

[22], which agree) and the total ionization measurements of Ref. [21] (cf. Fig. 10). In principle, these extra ions could be formed by positron-induced dissociation if the positron were to bind the dissociated, excited-state $O(^1D)$ oxygen atom. However in that case, the ion would be produced by annihilation, and hence measured in the current Ps formation measurements (i.e., as a lost positron).

In principal, the positive ion signal in the data of Ref. [21] might also have a component formed when the electronically excited $O(^1D)$ atoms from the neutral dissociation process strike the hemispherical scattering cell used in this experiment. The difference between the total ionization signal and the current Ps formation measurements in this energy range would then be proportional to the cross section for positron-induced dissociation. It appears, however, that the excitation energy of $O(^1D)$ (i.e., 2 eV) is too small for this scenario to be likely. Thus in our view, there is an unresolved discrepancy as to the origin of the excess ion signal reported in Ref. [21] relative to the current Ps formation measurements and those in Ref. [22] in the region from 7 to 12 eV.

C. Electronic excitation: N_2 and CO

The cross section for electronic excitation of N_2 by positron impact was measured previously by Sullivan *et al.* [12]. More detailed data for the $a\ ^1\Pi$ state ($E_{ex} = 8.59$ eV) in N_2 are shown in Fig. 11. The results for the $a'\ ^1\Sigma$ state ($E_{ex} = 8.40$ eV) of N_2 are shown in Fig. 12. Shown, for comparison, are the cross sections for the analogous electron impact cross sections [24,25]. Also shown in Fig. 11 are the most recent theoretical results for the positron excitation of the $a\ ^1\Pi$ state cross sections from Ref. [26].

The $a\ ^1\Pi$ state positron-impact cross section has a sharp onset, which is not observed in the analogous electron-
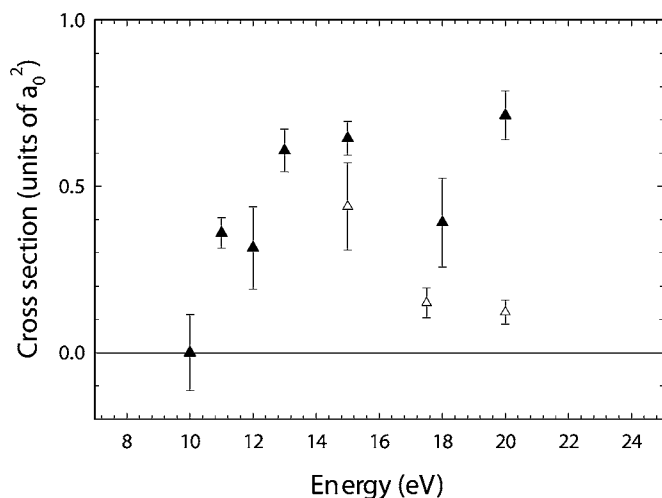
FIG. 12. Integral cross sections in N_2 for the excitation of the a' $^1\Sigma$ state by (▲) positrons (present data) and (△) electrons (from Ref. [24]).

FIG. 13. Integral cross sections for the excitation of the A $^1\Pi$ state in CO by (●) positron and (□) electron impact [28]. Also shown (—) is a theoretical calculation for the excitation of the A $^1\Pi$ state in CO by electrons [29].

impact cross section. While resonance features are ubiquitous in electron scattering, they have remained relatively elusive in positron scattering. This particular feature in N_2 and a similar one shown below for CO are two of the very few potential examples of resonances in positron scattering.

The recent theoretical calculation [26], shown in Fig. 11, does not show evidence of this feature. This calculation was performed using the Schwinger multichannel method. While this calculation does contain all of the open electronic states, it does not include the positronium formation channel. This channel opens at 8.78 eV (i.e., very near the threshold for the a $^1\Pi$ state at 8.59 eV), and so it may be that including this process is necessary. The three theoretical curves in the figure correspond to performing the calculation using three different basis sets for the N_2 molecule: Hartree Fock orbitals, mixed bonding orbitals, and mixed antibonding orbitals (ABOs). The authors of Ref. [26] indicate that, while the ABO calculation best matches the data as expected, the large variation of three results raise some question as to the accuracy of the calculations [27].

In Fig. 13 are shown cross section data for the A $^1\Pi$ state ($E_{ex}=8.07$ eV) in CO. There is a sharp turnon at threshold, and the maximum value is about twice that for N_2. Also shown, for comparison, are the analogous experimental and theoretical electron-impact cross sections [28,29].

Figure 14 shows a comparison of the results for electronic excitation and positronium formation in N_2 and CO. It is likely that the relative magnitudes of the a $^1\Pi$ electronic excitation cross section and the positronium formation cross section in N_2 at about 9–10 eV explains why it is the most effective buffer gas identified to date for positron trapping (i.e., in terms of high trapping efficiency). As compared with CO, for example, the ratio of the near-threshold electronic excitation cross section to the positronium formation cross section is >1 for N_2 but ≤ 1 for CO. This may be due to the fact that, in N_2, the electronic excitation channel is open before the positronium formation channel; whereas for the reverse is true for CO and most other atomic and molecular species.
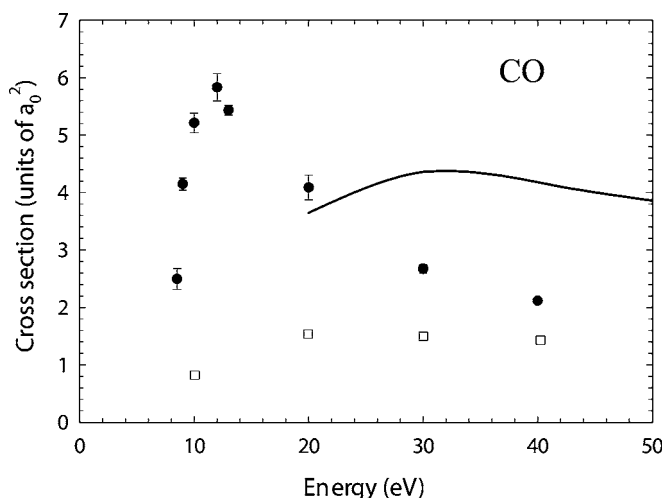
It has long been recognized that N_2 is the most efficient buffer gas for positron trapping and that the efficiency is maximized when the various trap stages are tuned to correspond to a positron energy loss of 9 eV per collision [5,6]. The likely explanation is the relatively large electronic excitation cross section of the a $^1\Pi$ state relative to the cross section for positronium formation in N_2.

IV. SUMMARY

This paper presents results for positronium formation in N_2 and CO. Also presented are results for the total and direct ionization cross sections for both these targets and O_2. Figure
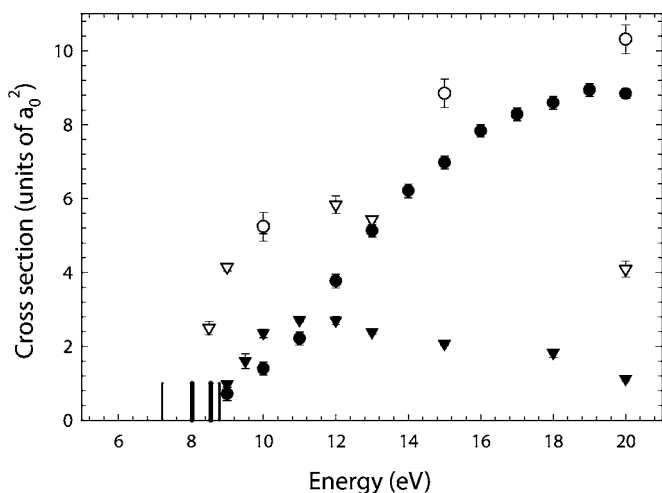

FIG. 14. Comparison of the electronic excitation (▼, ▽) and positronium formation (●, ○) cross sections in N_2 (solid) and CO (open). The vertical bars on the x axis mark the threshold values for Ps formation in CO, electronic excitation in CO, electronic excitation in N_2, and Ps formation in N_2, respectively.
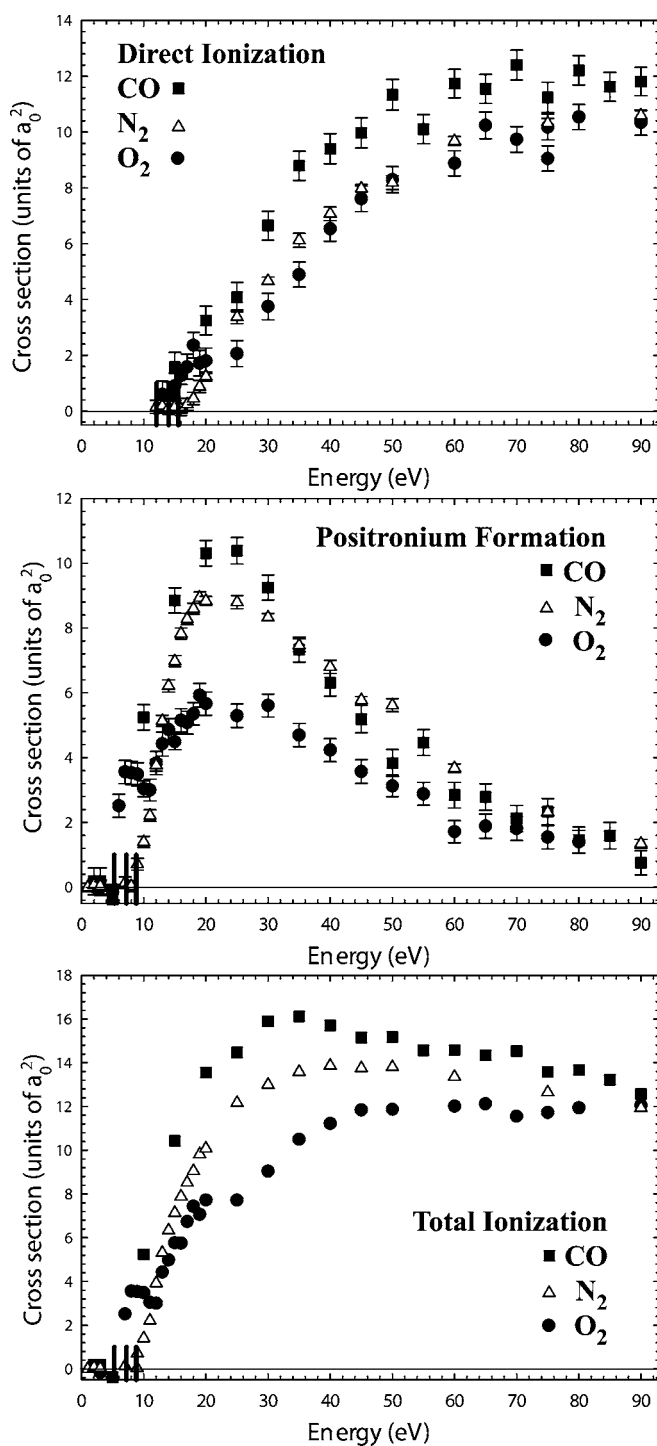
FIG. 15. Integral cross sections for the direct ionization, positronium formation, and total ionization of CO, N_2, and O_2, respectively. Vertical bars mark the positions of the thresholds for O_2, CO, and N_2, respectively.

15 shows a comparison of the cross sections for the three molecules. The isoelectronic molecules N_2 and CO have similar positronium formation and ionization cross sections as might be expected. However, the positronium formation cross section for O_2 is qualitatively different near threshold from those for N_2 and CO.

The characteristic shape of the near-threshold feature in O_2 has qualitative similarities to a feature observed previously in the total ionization cross section for O_2 in this region of energies. In that work, it was attributed to the onset of the excitation of the Schumann-Runge continuum in O_2 (i.e., breakup of the neutral molecule into atomic oxygen) which has a threshold just above the positronium formation threshold.

There is good agreement between the present measurements for the direct ionization cross sections in N_2 and CO and those of Refs. [16,17]. It is interesting to note that the direct ionization cross sections for these targets by electron impact are almost identical from 50 to 90 eV [30], which is not the case for the positron-impact measurements presented here or those of Refs. [16,17]. In CO, the total positron-impact ionization cross sections presented here are also in good agreement with those of Ref. [17]. In N_2, the results for total ionization are significantly lower than the previous measurements of Ref. [16].

In O_2, there is good agreement between the current experimental data for Ps formation and previous experimental data below the direct ionization threshold, but a significant disagreement in the cross section above this threshold. An independent measure of the Ps formation cross section in this region was presented which supports the current measurements. There is good agreement between the present measurements of the total ionization cross section and previous measurements above the direct ionization threshold, but significant disagreement between the two sets of measurements below this threshold. The possible explanation of this discrepancy, which would appear to be an excess positive ion signal that does not involve the disappearance of a positron, is not readily apparent. The agreement between the two existing experimental direct-ionization measurements for O_2 is good. However, neither of the two sets of experimental direct ionization measurements agree well with a recent theoretical calculation.

While there is a good degree of consensus, at least among experimental results, for the cross sections in N_2 and CO, this is not the case for O_2 at low energies. Further experimental examination of the cross sections for this target is warranted. Of particular interest is understanding the potential role of positron-induced dissociation, which appears as if it may be important at energies between the positronium formation threshold and that for direct ionization. Improved theoretical calculations for direct ionization would be welcome. Theoretical predictions for the positronium formation cross sections for all molecules studied would also be of great interest.

In the case of electronic excitation, there are many similarities between the cross sections in N_2 and CO, including a rapid rise at threshold for excitation of the $^1\Pi$ electronic state. Comparison of the electronic excitation and positronium formation cross sections in N_2, indicates that the likely reason N_2 is the most efficient buffer gas for positron trapping is the larger cross section for electronic excitation, as compared to that for positronium formation, in the range from 9 to 11 eV.

ACKNOWLEDGMENTS

[1] J. P. Marler, J. P. Sullivan, and C. M. Surko, Phys. Rev. A **71**, 022701 (2005).

[2] R. I. Campeanu, V. Chis, L. Nagy, and A. D. Stauffer, Nucl. Instrum. Methods Phys. Res. B **221**, 21 (2004).

[3] R. I. Campeanu, V. Chis, L. Nagy, and A. D. Stauffer, Phys. Lett. A **325**, 66 (2004).

[4] M. Charlton and J. Humberston, *Positron Physics* (Cambridge University Press, New York, 2001).

[5] T. J. Murphy and C. M. Surko, Phys. Rev. A **46**, 5696 (1992).

[6] C. M. Surko, A. Passner, M. Leventhal, and F. J. Wysocki, Phys. Rev. Lett. **61**, 1831 (1988).

[7] S. J. Gilbert, C. Kurz, R. G. Greaves, and C. M. Surko, Appl. Phys. Lett. **70**, 1944 (1997).

[8] C. Kurz, S. J. Gilbert, R. G. Greaves, and C. M. Surko, Nucl. Instrum. Methods Phys. Res. B **143**, 188 (1998).

[9] S. J. Gilbert, R. G. Greaves, and C. M. Surko, Phys. Rev. Lett. **82**, 5032 (1999).

[10] J. P. Sullivan, S. J. Gilbert, J. P. Marler, R. G. Greaves, S. J. Buckman, and C. M. Surko, Phys. Rev. A **66**, 042708 (2002).

[11] J. P. Sullivan, S. J. Gilbert, and C. M. Surko, Phys. Rev. Lett. **86**, 1494 (2001).

[12] J. P. Sullivan, J. P. Marler, S. J. Gilbert, S. J. Buckman, and C. M. Surko, Phys. Rev. Lett. **87**, 073201 (2001).

[13] G. Laricchia, P. V. Reeth, M. Szluińska, and J. Moxom, J. Phys. B **35**, 2525 (2002).

[14] W. Benesch, J. T. Vanderslice, S. G. Tilford, and P. G. Wilkinson, Astrophys. J. **143**, 236 (1966).

[15] D. C. Cartwright (private communication via M. J. Brunger).

[16] H. Bluhme, N. P. Frandsen, F. M. Jacobsen, H. Knudesn, J. Merrison, K. Paludan, and M. R. Poulsen, J. Phys. B **31**, 4631 (1998).

[17] H. Bluhme, N. P. Frandsen, F. M. Jacobsen, H. Knudesn, J. Merrison, K. Paludan, and M. R. Poulsen, J. Phys. B **32**, 5825 (1999).

[18] R. I. Campeanu, V. Chis, L. Nagy, and A. D. Stauffer, Phys. Lett. A **344**, 247–252 (2005).

[19] G. Herzberg, *Molecular Spectra and Molecular Structure I. Spectra od Diatomic Molecules* (Van Nostrand Reinhold Company, New York, 1950).

[20] Y. Katayama, O. Sueoka, and S. Mori, J. Phys. B **20**, 1645 (1987).

[21] G. Laricchia, J. Moxom, and M. Charlton, Phys. Rev. Lett. **70**, 3229 (1993).

[22] T. C. Griffith, in *Positron Scattering in Gases*, edited by J. W. Humberston and M. R. C. McDowell (Plenum Press, New York, 1983), pp. 53–63.

[23] K. P. Huber and G. Herzberg, *Constants of Diatomic Molecules* (Van Nostrand Reinhold Company, New York, 1979).

[24] L. Campbell, M. J. Brunger, A. M. Nolan, L. J. Kelly, A. B. Wedding, J. Harrison, P. J. O. Teubner, D. C. Cartwright, and B. McLaughlin, J. Phys. B **34**, 1185 (2001).

[25] N. J. Mason and W. R. Newell, J. Phys. B **20**, 3913 (1987).

[26] P. Chaudhuri, M. T. doN. Varella, C. R. C. deCarvalho, and M. A. P. Lima, Phys. Rev. A **69**, 042703 (2004).

[27] M. A. P. Lima (private communication).

[28] J. M. Ajello, J. Chem. Phys. **55**, 3158 (1971).

[29] M.-T. Lee, A. M. Machado, M. M. Fujimoto, L. E. Machado, and L. M. Brescansin, J. Phys. B **29**, 4285 (1996).

[30] R. S. Freund, R. C. Wetzel, and R. J. Shul, Phys. Rev. A **41**, 5861 (1990).